IEEE Access
Multidisciplinary | Rapid Review | Open Access Journal

IEEE POWER & ENERGY SOCIETY SECTION

Received March 7, 2021, accepted March 18, 2021, date of publication March 23, 2021, date of current version April 1, 2021.

Digital Object Identifier 10.1109/ACCESS.2021.3068193

Coordinated Control Between Prevention and Correction of AC/DC Hybrid Power System Based on Steady-State Security Region

ZHONG CHEN, (Member, IEEE), JUN YAN, (Student Member, IEEE), AND CHEN LU, (Student Member, IEEE)
School of Electrical Engineering, Southeast University, Nanjing 210096, China

Corresponding author: Jun Yan (yanj_hn@foxmail.com)

This work was supported in part by the National Key Research and Development Program of China under Grant 2016YFB0900602, and in part by the Technology Projects of State Grid Corporation of China under Grant 52094017000W.

ABSTRACT Taking the Steady-state Security Region (SSR) of AC/DC hybrid power system as a link, the mathematical model of coordinated control optimization problem is established by using the complementarity between preventive control and corrective control. Firstly, taking into account the probability and severity of anticipated accidents, a two-layer optimization model of coordinated control with dynamic constraints is established with the lowest total cost of coordinated control as the objective function. Secondly, invalid anticipated accidents are eliminated based on the theory of dominant event, which reduces the scale of the model and the complexity of optimization space. Finally, based on the constraint relaxation outer-layer optimization method, the anticipated accident with the minimum Steady-state Security Distance(SSD) is eliminated from the preventive control subset and incorporated into the corrective control subset, providing fixed anticipated accident subsets for the inner-layer optimization. In the inner-layer optimization, the SSDs are used to replace the power flow equations as the constraint condition, then the nonlinear constraints are transformed into linear constraints, which can reduce the difficulty of solving the mathematical model. The transformed IEEE 39 node AC/DC hybrid system is analyzed and calculated, and the calculation results verify that the proposed method can effectively improve the efficiency of solving optimal control scheme, and provide the possibility for online application.

INDEX TERMS AC/DC hybrid power system, steady-state security region, coordinated control, dominant event, constraint relaxation.

I. INTRODUCTION

Nowadays, the power system is developing towards the direction of large power grid and AC/DC hybrid connection, and its operating environment is more and more complex, which makes the issue of static security of the power grid more challenging than ever, and the study of power system security control is becoming more and more important [1]–[4]. Preventive control and corrective control are two commonly used security control methods, however, large-scale AC/DC hybrid power systems may have many anticipated accidents in the future, and their severity and probability vary greatly. When designing a control scheme, if only preventive control or corrective control is used to ensure the static security of all anticipated accidents at the same time, the control cost may be too high or the control scheme may be practically unfeasible. While preventive control and corrective control have strong complementary in physical and economic characteristics, the coordination between them is an important element in the field of static security control in AC/DC hybrid power system [5]–[8].

The control time of preventive control and corrective control can be divided into before and after these accidents. Therefore, it is necessary to classify these anticipated accidents first and decompose the security control pressure into before and after of these accidents. In [9], based on the single-machine equivalent theory, the anticipated accidents were classified according to their severity, but probabilities of these accidents are ignored; Wang *et al.* [10] considered the severity and probability of anticipated accidents firstly and then

The associate editor coordinating the review of this manuscript and approving it for publication was S. Srivastava.

used the golden section search to classify these anticipated accidents. Other researchers [11], [12] used the risk index to classify these anticipated accidents, but the selection of the risk index depended on the operation experience of the dispatcher so it is highly subjective.

After classifying these anticipated accidents, it is necessary to formulate a corresponding control scheme for these determined accident subsets. Verma *et al.* [13] proposed a preventive control of transient stability with generation rescheduling based on coherency obtained from time domain simulations. Alzaareer *et al.* [14] used the sensitivity analysis to select the most effective control variables to maintain the voltage stability of the system. Zhou *et al.* [6] proposed a chaos particle swarm optimization (CPSO) algorithm combined with particle mining algorithm to formulate a control scheme to maintain the stability of the system. However, these above formulating methods of control strategy mainly rely on complex simulation calculations. The large amount of calculation makes it difficult to apply online, and it is difficult to master the overall security statue of the system during adjustment.

The Steady-state Security Region (SSR) describes the overall security operation region, which is only related to the network topology and constraints of the system, and has nothing to do with the operating state of the system, therefore, the SSR can be calculated offline and applied online. Besides, within the scope of engineering concern, the practical boundary surfaces of SSR in the decision space can be approximated by a few hyperplanes. Whether the current operation state is security or not can be judged by observing the relative position relationship between the operating point and the boundary surfaces of SSR. The safety margin and optimal control information of the system can also be obtained by observing the Steady-state Security Distance (SSD) between the operating point and the boundary surfaces of SSR [15]–[17]. At the same time, using the boundary surfaces of the SSR represented by hyperplanes as the constraint condition, the constraint condition can be transformed into linear combination inequality constraint, which makes the difficult problem of stability-constrained dealing with optimization problem become very simple, and provides the possibility for online application. At present, SSR has achieved good application results in power system risk assessment [18], [19], optimal power flow [20], [21] and security control [22], [23].

Based on the above analysis, this paper proposed a coordinated control optimization model based on SSR. The advantages of the coordinated control method and the main contributions of this paper can be listed as follows:

1) Based on the theory of SSR of AC/DC hybrid power system, the boundary surfaces of SSR are represented by hyperplanes, and the calculation methods of expressions of hyperplanes and SSD are provided.

2) Based on the theory of dominant event, these invalid anticipated accidents are eliminated so the scale of the model is reduced. And then use the constraint relaxation outer-layer optimization method to classify these screened anticipated accidents, provide fixed anticipated accident subsets for the inner-layer optimization, decompose the security control pressure into before and after of these accidents.

3) When carrying out the inner-layer optimization for these given anticipated accident subsets, the probability and severity of anticipated accidents are considered comprehensively, and the constraint conditions are simplified by taking the SSD as the constraint condition, thus the optimal coordinated control scheme can be solved quickly and provide the possibility for online application.

II. MODEL OF STEADY-STATE SECURITY REGION OF AC/DC HYBRID POWER SYSTEM

A. STEADY-STATE SECURITY REGION IN CONTROL VARIABLE SPACE

The SSR of AC/DC hybrid system is a region that satisfies the system equality constraint and inequality constraint in the control variable space. Suppose there are only two control variables x_α^1 and x_α^2, two state variables x_β^1 and x_β^2 in the system, and the SSR as shown in the shaded part in Figure 1. $\boldsymbol{x_\alpha}(x_\alpha^1, x_\alpha^2)$ corresponding to any point inside this region (e.g., point a) is security when verified by the point-wise method. And $\boldsymbol{x_\alpha}(x_\alpha^1, x_\alpha^2)$ corresponding to any point outside this region (e.g., point b) is insecurity when verified by the point-wise method.

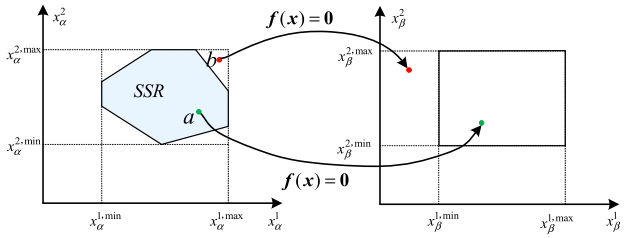

FIGURE 1. The connection between SSR method and point-wise method.

The SSR defined in the control variable space is the set of all operating points $\boldsymbol{x}_\alpha$ that satisfy the equality and inequality constraints, which can be expressed as follows:

$$\Omega \triangleq \boldsymbol{x}_\alpha \in \boldsymbol{R}^n | \forall \boldsymbol{x} = (\boldsymbol{x}_\alpha, \boldsymbol{x}_\beta) \text{ satisfy} \quad \boldsymbol{f}(\boldsymbol{x}) = \boldsymbol{0},\ \boldsymbol{g}(\boldsymbol{x}) \leq \boldsymbol{0} \tag{1}$$

where, $\boldsymbol{x}_\alpha = \{x_\alpha^1, x_\alpha^2, \cdots, x_\alpha^n\}$ denotes the control variables of AC/DC hybrid system, e.g., the control variables of DC subsystem, active output and voltage amplitude of PV nodes, active load and reactive load of PQ nodes; n denotes the number of control variables, which also denotes the geometric dimension of the SSR; $\boldsymbol{R}^n$ denotes the n-dimensional Euclidean geometric space; $\boldsymbol{x}_\beta = \{x_\beta^1, x_\beta^2, \cdots, x_\beta^n\}$ denotes the state variables of AC/DC hybrid system, e.g., upper and lower limits of line power flow and voltage amplitude of PQ nodes; $\boldsymbol{f}(\boldsymbol{x}) = \boldsymbol{0}$ denotes equality constraint equations and $\boldsymbol{g}(\boldsymbol{x}) \leq \boldsymbol{0}$ denotes inequality constraint equations.

For a given system network topology and system parameters, the SSR is uniquely determined, and the internal of SSR is connected and empty, which is independent of the operating

state of the system. Therefore, the SSR can be calculated offline and applied online [17]. At the same time, when the reactive power of the converter station is compensated locally, the boundary surface of SSR in the high-dimensional Euclidean geometric space can be approximately described by the hyperplane within the scope of Engineering permission. The boundary surfaces of SSR represented by the linear expressions simplify the constraints of the system in optimal control problem, and provides the possibility for online control scheme formulation.

B. LINEAR EXPRESSION OF SSR BOUNDARY SURFACE

The boundary surfaces of SSR in high-dimensional Euclidean geometric space is mainly composed of two parts: The operation constraint region Ω_r surrounded by operation constraint boundary surface B_r composed of upper and lower limits of state variables; The security constraint region Ω_s surrounded by security constraint boundary surface B_s which is perpendicular to the coordinate axis and composed of upper and lower limits of control variables. The intersection Ω of them is SSR, as shown in the shaded part of Figure 2.

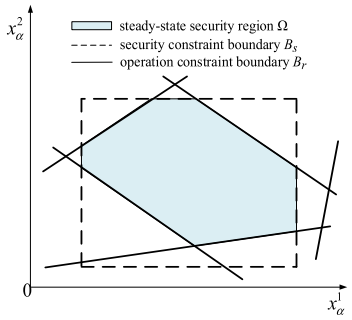

FIGURE 2. Diagram of Steady-state Security Region (SSR).

It can be seen from the definition of SSR that each inequality constraint in the equation (1) corresponds to a boundary surface of SSR. When an inequality constraint is transformed into an equality constraint and the rest of the equality and inequality constraints are still satisfied, the boundary surface corresponding to the inequality is formed. For example, for the upper voltage limit of the i-th PQ node, the corresponding boundary surface can be expressed as follows:

$$B_i = \{\boldsymbol{x}_\alpha \in \Omega | U_i = U_i^{\max}\} \tag{2}$$

Since the security constraint boundary surface B_s is perpendicular to the coordinate axis and corresponds to the upper and lower limits of the control variables, its expression can be obtained directly. However, the operation constraint boundary surface B_r is corresponding to the state variable constraint, and the expression calculation methods usually include analytical method and fitting method [23]. The analytical method is based on the DC power flow model to derive the expression of the surface, although the accuracy of analytical method is not high, it has the advantage of high efficiency. So the analytical method is usually suitable for the distribution network with frequent changes in network topology; The fitting method is based on the AC power flow model to calculate a certain number of critical points on the boundary surface B_r by the point-wise method, then normalizes these critical points with different dimensions, after that computes the linear expression of the fitting boundary surface of these critical points. Although the accuracy of fitting method is high, it needs to calculate a certain number of critical points, it has the disadvantage of low efficiency, so the fitting method is usually suitable for the transmission network with constant network topology. And the fitting coefficients of the boundary surface can be calculated offline and then applied online.

In this paper, the AC/DC hybrid power system with high voltage level is mainly studied, so the fitting method is used to calculate the expression of the boundary surface. At the same time, in order to ensure the uniform search direction of the critical points in the control variable space, the Hadamard orthogonal table is used to generate the search direction [24], [25] when searching the critical points, therefore, the solution process of expression of the constraint boundary surface B_r is shown in Figure 3.

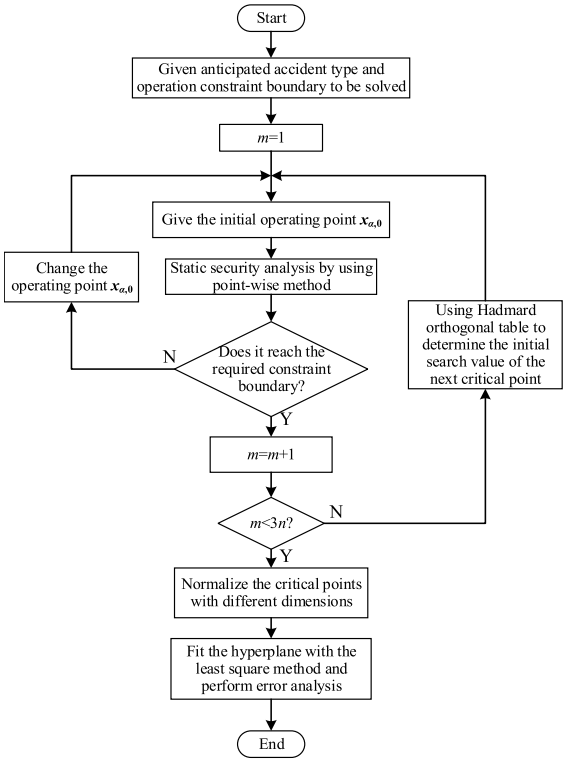

FIGURE 3. The flow chart for solving the expression of operation constraint boundary surface.

In Figure 3, n denotes the dimension of the SSR, which also denotes the number of control variables; m denotes the number of critical points searched. In order to ensure the fitting effect for each boundary surface, the number of critical points is 3 times the dimension of the number of control variables.

Assuming that the rectifier side of the DC subsystem adopts constant current control and the inverter side adopts constant voltage control, the t-th mathematical expression of the operation constraint boundary $B_{r,t}$ can be expressed as follows:

$$\sum_{i\in G}(\alpha_{t,i}P_{\mathrm{G}i}+\beta_{t,i}V_{\mathrm{G}i})+\sum_{j\in L}(\eta_{t,j}P_{\mathrm{L}j}+\lambda_{t,j}Q_{\mathrm{L}j})+\sum_{m\in D}(\mu_{t,m}I_{\mathrm{d}m}+\omega_{t,m}U_{\mathrm{inv}m})=a_0 \quad (3)$$

where, G, L, D denote the set of PV nodes (except the balance node), PQ nodes, and DC lines; $\alpha_{t,i}$, $\beta_{t,i}$, $\eta_{t,j}$, $\lambda_{t,j}$, $\mu_{t,m}$, $\omega_{t,m}$ denote the fitting coefficient of the boundary surface $B_{r,t}$; $P_{\mathrm{G}i}$, $V_{\mathrm{G}i}$ denote the active power output and voltage amplitude of the i-th PV node; $P_{\mathrm{L}j}$, $Q_{\mathrm{L}j}$ denote the active power load and reactive power load of the j-th PQ node; $I_{\mathrm{d}m}$, $U_{\mathrm{inv}m}$ denote the constant current value of rectifier side and the constant voltage value of inverter side of the m-th DC line, and a_0 denotes the observation variable, usually $a_0 = 1$.

Expanding the equation (3), the linear expression of boundary surface $B_{r,t}$ can be obtained, it can be expressed as follows:

$$a_{t,1}x_\alpha^1+a_{t,2}x_\alpha^2+\cdots+a_{t,n}x_\alpha^n=a_0 \quad (4)$$

where, n denotes the dimension of the SSR, $x_\alpha^i(i=1,2,\cdots,n)$ denotes the control variable of the system, which also denotes the dimension variable of the SSR, $a_{t,i}(i=1,2,\cdots,n)$ denotes the coefficient of the boundary surface $B_{r,t}$.

For the linear fitting effect of the operation constraint boundary surface $B_{r,t}$, the fitting error e_{rr} can be used to characterize it. In general, when the fitting error of all critical points are not more than 5%, it can be considered to meet the engineering requirements. The smaller the fitting error e_{rr} is, the higher the accuracy is [26]. The fitting error of critical point $\boldsymbol{x}_{\boldsymbol{\alpha},j}=(x_{\alpha,j}^1,x_{\alpha,j}^2,\cdots,x_{\alpha,j}^n)$ on boundary surface $B_{r,t}$ can be expressed as follows:

$$err_j=\frac{|a_{t,1}x_{\alpha,j}^1+a_{t,2}x_{\alpha,j}^2+\cdots+a_{t,n}x_{\alpha,j}^n-a_0|}{\sqrt{a_{t,1}^2+a_{t,2}^2+\cdots+a_{t,n}^2}\times\sqrt{\sum_{i=1}^n(x_{\alpha,j}^i)^2}} \quad (5)$$

where $\sqrt{\sum_{i=1}^n(x_{\alpha,j}^i)^2}$ denotes the distance from the critical point $\boldsymbol{x}_{\boldsymbol{\alpha},j}$ to the origin.

C. STEADY-STATE SECURITY DISTANCE

On the theory of SSR, scholars have designed different indicators to characterize the security and security margin of the system. The SSD is one of the representative indicators [16], [27].

Suppose the current operating point of the system is $\boldsymbol{x}_{\alpha,0}=(x_{\alpha,0}^1,x_{\alpha,0}^2,\cdots,x_{\alpha,0}^n)$, then in the n-dimensional Euclidean geometric space $\boldsymbol{R}^n$, the SSD from $\boldsymbol{x}_{\alpha,0}$ to the boundary surface $B_{r,t}$ can be expressed as follows:

$$d_t=\frac{a_{t,1}x_{\alpha,0}^1+a_{t,2}x_{\alpha,0}^2+\cdots+a_{t,n}x_{\alpha,0}^n-a_0}{\sqrt{a_{t,1}^2+a_{t,2}^2+\cdots+a_{t,n}^2}} \quad (6)$$

where, the absolute value sign of the molecule is removed, so the d_t is a signed value. The positive and negative can represent the relative position relationship between the operating point $\boldsymbol{x}_{\alpha,0}$ and the boundary surface $B_{r,t}$, that is, whether it is located inside or outside the SSR, so as to represent the security of the system.

The method to judge the security of the operating point is as follows: for the upper-limit constraint boundary surface B_{up}, the sufficient and necessary condition of the operating point in the SSR is $d_t < 0$; on the contrary, for the lower-limit constraint boundary surface B_{down}, the sufficient and necessary condition of the operating point in the SSR is $d_t > 0$. The greater the absolute value d_t is, the closer it is to the center of the SSR, and the safer the system will be. The coordinate point $(0.5, 0.5, \cdots, 0.5)$ can be considered as the geometric center of the SSR.

III. COORDINATION CONTROL BASED ON SSR

For a large-scale AC/DC hybrid power system, there are many anticipated accidents, and the possibility of each accident and the economic loss caused by each accident are also different. If only preventive control is used to ensure the security of the system, low probability accidents will increase the cost of preventive control. If only corrective control is used to ensure the security of the system, high probability accidents will increase the expected dispatching cost and risk cost of corrective control. However the preventive control before the accidents and the corrective control after the accidents are highly complementary in physical and economic characteristics, if the preventive control and the corrective control are respectively responsible for the static security of part of these accidents, the total security control cost may be reduced.

A. THE IDEA OF COORDINATED CONTROL BASED ON SSR

The coordinated control process of AC/DC hybrid power system based on SSR is divided into three steps:

Step 1: Divide the anticipated accident set Γ into preventive control subset Γ_p and corrective control subset Γ_c. The static security of Γ_p is ensured by preventive control, and the static security of Γ_c is ensured by corrective control.

Step 2: Formulate a preventive control scheme $\Delta\boldsymbol{x}_{\alpha,p}$ to move the initial operating point $\boldsymbol{x}_{\alpha,0}\notin\bigcap_{\lambda_i\in\Gamma_p}\Omega(\lambda_i)\in\boldsymbol{R}^n$ of the system to $\boldsymbol{x}_{\alpha,p}\in\bigcap_{\lambda_i\in\Gamma_p}\Omega(\lambda_i)\in\boldsymbol{R}^n$, that is, within the intersection of the SSR of the preventive control subset Γ_p.

Step 3: Formulate a corrective control scheme $\Delta\boldsymbol{x}_{\alpha,cj}$ for each anticipated accident $\lambda_j(\lambda_j\in\Gamma_c)$ in Γ_c, and move the operating point $\boldsymbol{x}_{\alpha,p}$ after the preventive control from $\boldsymbol{x}_{\alpha,p}\notin\Omega(\lambda_j)\in\boldsymbol{R}^n$ to $\boldsymbol{x}_{\alpha,cj}\in\Omega(\lambda_j)\in\boldsymbol{R}^n$, thus forming the corrective control scheme set $\Delta\boldsymbol{x}_{\alpha,c}=\{\Delta\boldsymbol{x}_{\alpha,c1},\Delta\boldsymbol{x}_{\alpha,c2},\cdots,\Delta\boldsymbol{x}_{\alpha,cj}\}^T$.

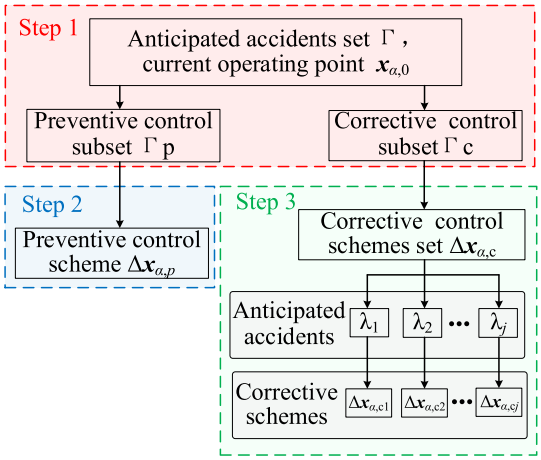

FIGURE 4. The diagram of coordinated control between prevention and correction.

The schematic diagram of coordinated control is shown in Figure 4.

After the implementation of preventive control, the system still needs to meet certain security margin under normal operating conditions. For the convenience of explanation, this paper takes the normal operation state as a special case of the preventive control subset Γ_p.

B. MATHEMATICAL MODEL OF COORDINATED CONTROL

From the economic point of view, the solution of coordinated control target operation point needs to consider the dispatching cost of preventive control before the accident, the expected dispatching cost and risk cost of corrective control after the accident. Therefore, this paper mainly considers the following three aspects of cost: dispatching cost of preventive control, expected dispatching cost and risk cost of corrective control.

1) THE DISPATCHING COST OF PREVENTIVE CONTROL

The purpose of preventive control is to pull the current operating point $\boldsymbol{x}_{\alpha,0}$ of the system to the intersection of SSR of the preventive control subset Γ_p. Therefore, the dispatching cost $C_p^d(\boldsymbol{x}_{\alpha,0}, \boldsymbol{x}_{\alpha,p})$ of preventive control can be expressed as follows:

$$C_p^d(\boldsymbol{x}_{\alpha,0}, \boldsymbol{x}_{\alpha,p}) = \boldsymbol{C}^T \cdot |\boldsymbol{x}_{\alpha,p} - \boldsymbol{x}_{\alpha,0}| \tag{7}$$

where: $\boldsymbol{C} = [c_1, c_2, \cdots, c_n]$ denotes the unit adjustment cost of each dimension variable of SSR; $\boldsymbol{x}_{\alpha,p} = [x_{\alpha,p}^1, x_{\alpha,p}^2, \cdots, x_{\alpha,p}^n]$ denotes the operating point after preventive control.

2) THE EXPECTED DISPATCHING COST OF CORRECTIVE CONTROL

The purpose of the corrective control is to formulate a corrective control measure $\Delta \boldsymbol{x}_{\alpha,cj}$ for each anticipated accident $\lambda_j(\lambda_j \in \Gamma_c)$ in Γ_c, and pull the operation point $\boldsymbol{x}_{\alpha,p}$ after preventive control to the $\Omega(\lambda_j)$, and then form the corrective control measures set $\Delta \boldsymbol{x}_{\alpha,c}$. For example, for the anticipated accident λ_j, the expected dispatching cost $C_c^d(\boldsymbol{x}_{\alpha,p}, \boldsymbol{x}_{\alpha,cj})$ of corrective control can be expressed as follows:

$$C_c^d(\boldsymbol{x}_{\alpha,p}, \boldsymbol{x}_{\alpha,cj}) = P(\lambda_j) \cdot \boldsymbol{C}^T \cdot |\boldsymbol{x}_{\alpha,cj} - \boldsymbol{x}_{\alpha,p}| \tag{8}$$

where: $\boldsymbol{x}_{\alpha,cj} = [x_{\alpha,cj}^1, x_{\alpha,cj}^2, \cdots, x_{\alpha,cj}^n]$ denotes the operation point after corrective control for the anticipated accident λ_j, $P(\lambda_j)$ denotes the probability of the anticipated accident $\lambda_j(\lambda_j \in \Gamma_c)$.

Furthermore, the expected dispatching cost $C_c^d(\boldsymbol{x}_{\alpha,p}, \boldsymbol{x}_{\alpha,c})$ of corrective control can be expressed as follows:

$$C_c^d(\boldsymbol{x}_{\alpha,p}, \boldsymbol{x}_{\alpha,c}) = \sum_{\lambda_j \in \Gamma_c} C_c^d(\boldsymbol{x}_{\alpha,p}, \boldsymbol{x}_{\alpha,cj}) \tag{9}$$

3) THE RISK COST OF CORRECTIVE CONTROL

When the anticipated accident $\lambda_j(\lambda_j \in \Gamma_c)$ occurs, it maybe cause the node voltage or line power flow out-of-limit, which will endanger the security of the AC/DC hybrid power system. In order to characterize the harm degree of out-of-limit to the system before the corrective control takes effect, the risk of voltage and power flow out-of-limit are introduced into the cost of coordinated control. The mathematical model can be expressed as follows:

$$C_r(f) = \sum_{\lambda_j \in \Gamma_c} (R_v(\lambda_j) + R_l(\lambda_j)) \tag{10}$$

where: $R_v(\lambda_j)$ denotes the voltage out-of-limit risk cost caused by anticipated accident λ_j, $R_l(\lambda_j)$ denotes the power flow out-of-limit risk cost caused by anticipated accident λ_j.

a: THE RISK COST OF VOLTAGE OUT-OF-LIMIT

When the anticipated accident λ_j occurs, the voltage out-of-limit severity function $G_v(\lambda_j, m)$ of the m-th PQ node is defined as follows:

$$G_v(\lambda_j, m) = \begin{cases} \omega_m \left(\dfrac{|2V_{\lambda_j}(m) - [V_{\max}(m) + V_{\min}(m)]|}{2[V_{\max}(m) - V_{\min}(m)]} - \dfrac{1}{2} \right)^{e_v} \\ \quad V_{\lambda_j}(m) > V_{\max}(m) || V_{\lambda_j}(m) < V_{\min}(m) \\ 0 \qquad V_{\min}(m) \le V_{\lambda_j}(m) \le V_{\max}(m) \end{cases} \tag{11}$$

where: $V_{\lambda_j}(m)$ denotes the voltage value of the m-th node when the anticipated accident λ_j occurs, $V_{\max}(m)$ and $V_{\min}(m)$ denote the voltage upper and lower limits of the m-th node respectively, ω_m denotes the node importance coefficient, and e_v denotes the severity index factor of voltage out-of-limit, the larger the value of e_v is, the easier it is to identify the serious accident.

The system voltage out-of-limit severity index $E_v(\lambda_j)$ caused by accident λ_j can be expressed as follows:

$$E_v(\lambda_j) = \sum_{m \in N_B} G_v(\lambda_j, m) \tag{12}$$

where: N_B denotes all PQ nodes in the system.

Therefore, the risk cost $R_v(\lambda_j)$ of voltage out-of-limit when the anticipated accident λ_j occurs can be expressed as follows:

$$R_v(\lambda_j) = P(\lambda_j)E_v(\lambda_j) \tag{13}$$

b: THE RISK COST OF POWER FLOW OUT-OF-LIMIT

The power flow out-of-limit severity function $G_l(\lambda_j, n)$ of the n-th branch when the anticipated accident λ_j occurs is defined as follows:

$$G_l(\lambda_j, n) = \begin{cases} \omega_k \left[\dfrac{|P_{\lambda_j}(n)| - P_{\max}(n)}{P_{\max}(n)} \right]^{e_l} & P_{\lambda_j}(n) > P_{\max}(n) \\ 0 & P_{\lambda_j}(n) < P_{\max}(n) \end{cases} \tag{14}$$

where: $P_{\lambda_j}(n)$ denotes the power transmission of the n-th line when the anticipated accident λ_j occurs, $P_{\max}(n)$ denotes the power flow upper limit of the n-th line, ω_k denotes importance coefficient of line, and e_l denotes the severity index factor of power flow overload. The larger the value of e_l is, the easier it is to identify the serious accident.

The system power flow out-of-limit severity index $E_l(\lambda_j)$ caused by anticipated accident λ_j can be expressed as follows:

$$E_l(\lambda_j) = \sum_{n \in N_l} G_l(\lambda_j, n) \tag{15}$$

where: N_l denotes all lines in the system.

Therefore, the risk cost $R_l(\lambda_j)$ of power flow out-of-limit when the anticipated accident λ_j occurs can be expressed as follows:

$$R_l(\lambda_j) = P(\lambda_j)E_l(\lambda_j) \tag{16}$$

4) MATHEMATICAL MODEL OF COORDINATED CONTROL COST

The objective of optimal coordination control is to ensure the security of all anticipated accidents by preventive control and corrective control, and at the same time minimize the total cost of coordinated control. Therefore, the mathematical model of coordinated control can be expressed as follows:

$$\begin{aligned} \min\ & F(\boldsymbol{x}_{\alpha,0}, \boldsymbol{x}_{\alpha,p}, \boldsymbol{x}_{\alpha,c}, z) \\ & = C_p(\boldsymbol{x}_{\alpha,0}, \boldsymbol{x}_{\alpha,p}) + C_c(\boldsymbol{x}_{\alpha,p}, \boldsymbol{x}_{\alpha,c}, f) \\ & = C_p^d(\boldsymbol{x}_{\alpha,0}, \boldsymbol{x}_{\alpha,p}) + C_c^d(\boldsymbol{x}_{\alpha,p}, \boldsymbol{x}_{\alpha,c}) + C_r(f) \\ s.t.\ & \\ & |\boldsymbol{x}_{\alpha,cj} - \boldsymbol{x}_{\alpha,p}| \le k_i \Delta t \\ & \boldsymbol{x}_{\alpha,p} \in \bigcap_{\lambda_i \in \Gamma_p} \Omega(\lambda_i) \\ & \boldsymbol{x}_{\alpha,cj} \in \Omega(\lambda_j) \quad (\forall \lambda_j \in \Gamma_c) \\ & d_{\lambda_m,n} \le -d_{\min} \quad (\forall \lambda_m \in \Gamma, n \in B_{up}) \\ & d_{\lambda_m,n} \ge d_{\min} \quad (\forall \lambda_m \in \Gamma, n \in B_{down}) \end{aligned} \tag{17}$$

where: $C_p(\boldsymbol{x}_{\alpha,0}, \boldsymbol{x}_{\alpha,p})$ denotes the cost of preventive control, equal to dispatching cost $C_p^d(\boldsymbol{x}_{\alpha,0}, \boldsymbol{x}_{\alpha,p})$ of the preventive control; $C_c(\boldsymbol{x}_{\alpha,p}, \boldsymbol{x}_{\alpha,c}, z)$ denotes the expected cost of corrective control, including the expected dispatching cost $C_c^d(\boldsymbol{x}_{\alpha,p}, \boldsymbol{x}_{\alpha,c})$ and risk cost $C_r(f)$ of corrective control.

In the constraint condition of the Equation (17), the first equation denotes the coupling relationship between the corrective control and the preventive control, where k_i denotes the allowed adjustment rate of the i-th dimension variable in the SSR, and Δt is the allowed emergency adjustment time of corrective control. The second and third equations denote the system static security constraints represented by the SSR. $\bigcap_{\lambda_i \in \Gamma_p} \Omega(\lambda_i)$ denotes the intersection of SSR corresponding to the preventive control subset Γ_p, and $\Omega(\lambda_j)$ denotes the SSR corresponding to the anticipated accident λ_j. The fourth and the fifth equations denote the minimum stability margin constraint, where $d_{\lambda_m,n}$ denotes the SSD from the operating point to the boundary surface B_n of the anticipated accident λ_m, B_{up} and B_{down} denote the boundary surfaces corresponding to the upper limit and lower limit of the constraint respectively.

At last, anti-normalization of the solved operating points, the actual operating points of the system can be obtained.

IV. COORDINATED CONTROL OPTIMIZATION METHOD BASED ON SSR

It can be seen from the Figure 4 that the mathematical model of coordinated control is a two-layer optimization problem with dynamic constraints. The outer-layer optimization determines the dynamic change of constraints, which divides the anticipated accident set Γ into preventive control subset Γ_p and corrective control subset Γ_c, then provides fixed anticipated accident subsets for the inner-layer optimization. For the determined Γ_p and Γ_c, inner-layer optimization formulates preventive control scheme $\Delta \boldsymbol{x}_{\alpha,p}$ and corrective control scheme set $\Delta \boldsymbol{x}_{\alpha,c}$ with minimum total control cost.

The inner-layer optimization is the optimization problem shown in Equation (17). Since the equation (17) takes SSDs as the constraint condition, the inner-layer optimization of coordinated control is actually a typical linear programming problem, and the current algorithm has been quite mature.

For the outer-layer optimization, if the anticipated accidents set is small, the optimal solution can be obtained by exhaustive method. However, when the number of anticipated accidents is large, this method may bring ''curse of dimensionality'' and will become infeasible. Therefore, a new outer-layer optimization method is needed to solve the outer-layer optimization problem in a shortest possible time. Therefore, in this paper, these anticipated accidents are screened based on the theory of dominant event to reduce the model scale, and then, the constraint relaxation method for outer-layer optimization is proposed for the screened dominant events.

A. CONSTRAINT REDUCTION BASED ON DOMINANT EVENT THEORY

In a large-scale AC/DC hybrid power system, the number of anticipated accidents may be very large. If all anticipated accidents are considered, there are two problems as follows:

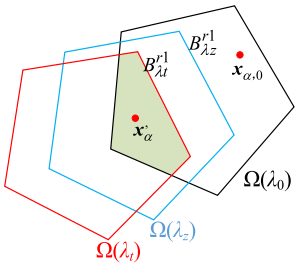

FIGURE 5. Schematic diagram of dominant event theory.

(1) Although the fitting method has high accuracy in solving the boundary surfaces of SSR, it also has the disadvantage of low efficiency. If the boundary surfaces of all anticipated accidents are depicted, the calculation amount is bound to increase; (2) If the boundary surface constraints of all anticipated accidents are considered, it will not only complicate the outer-layer optimization, but also complicate the optimization space of preventive control.

However, in the actual process, the number of valid anticipated accidents is not large. By using the theory of dominant event and screening these anticipated accidents, the number of valid anticipated accidents can be reduced and the scale of coordinated control model can be simplified too.

In the case of anticipated accident λ_t occurs, the out-of-limit value $Y^r_{\lambda t}$ of electrical quantity r can be expressed as follows:

$$Y^r_{\lambda t} = \max\ (0, |T_r| - T_r^{\max}) \tag{18}$$

where: T_r denotes the value of electrical quantity r, and the r includes the upper and lower limits of line power flow and node voltage.

The dominant event means that if the out-of-limit value of all electrical quantities caused by accident λ_t are larger than the corresponding out-of-limit value of electrical quantities caused by accident λ_z, namely:

$$Y^r_{\lambda t} \geq Y^r_{\lambda z}, \quad r = 1, 2, \cdots m \tag{19}$$

Then accident λ_t is termed as dominate accident λ_z, and accident λ_t is the dominant event, accident λ_z is the dominated event, If a new operation point meets the static security of accident λ_t, it must meet the static security of accident λ_z. And the theoretical basis of dominant event can be referred to [28], [29].

Taking the two-dimensional SSR as an example, assume that the SSR of normal operating conditions is $\Omega(\lambda_0)$ in Figure 5, and the initial operating point $\boldsymbol{x}_{\alpha,0}$ is located in $\Omega(\lambda_0)$, the SSRs corresponding to accidents λ_t and λ_z are respectively $\Omega(\lambda_t)$ and $\Omega(\lambda_z)$, and both of them will cause the electrical quantity r_1 to out-of-limit. And the out-of-limit value caused by accident λ_t is greater than the out-of-limit value caused by accident λ_z, so the distance $|d^{r1}_{\lambda t}|$ from $\boldsymbol{x}_{\alpha,0}$ to boundary surface $B^{r1}_{\lambda t}$ is greater than the distance $|d^{r1}_{\lambda z}|$ from $\boldsymbol{x}_{\alpha,0}$ to boundary surface $B^{r1}_{\lambda z}$.

If the operation point $\boldsymbol{x}^{'}_{\alpha}$ satisfies $\boldsymbol{x}^{'}_{\alpha} \in \Omega(\lambda_0) \cap \Omega(\lambda_t)$, then $\boldsymbol{x}^{'}_{\alpha}$ must satisfy $\boldsymbol{x}^{'}_{\alpha} \in \Omega(\lambda_0) \cap \Omega(\lambda_t) \cap \Omega(\lambda_z)$, as shown in the shadow of Figure 5. Therefore, the constraint corresponding to the $\Omega(\lambda_z)$ of the accident λ_z is invalid. In the coordinated control, the description of $\Omega(\lambda_z)$ can be ignored, which not only improves the efficiency of depiction for SSR, but also simplifies the scale of the model.

Therefore, by comparing the anticipated accidents with each other and eliminating the dominated anticipated accidents, the set of dominant anticipated accidents can be obtained. The specific process is as follows:

(1) Under the current operating state of the AC/DC hybrid power system, determine the initial anticipated accident set Γ_a, and calculate the power flow distribution of each anticipated accident, then obtain the measurement index of the transmission component out-of-limit under each anticipated accident;

(2) Compare the anticipated accidents in Γ_a, and get the set Γ_d of dominated anticipated accidents;

(3) Obtain $\Gamma = \Gamma_a - \Gamma_d$, and all anticipated accidents in Γ are valid anticipated accidents.

B. OUTER-LAYER OPTIMIZATION METHOD BASED ON CONSTRAINT RELAXATION

If the preventive control is responsible for all of these anticipated accidents in Γ, i.e. $\Gamma_p = \Gamma$, the cost of preventive control is the highest, while the expected cost of corrective control is the lowest. In order to reduce the total cost of coordinated control, the most serious accident (with minimum SSD after preventive control) in Γ_p can be eliminated from Γ_p and incorporated into Γ_c. In this case, the preventive control cost will decrease and the expected cost of corrective control will increase, but the increase or decreases of the total cost need to be further observed.

Based on the above analysis, the outer-layer optimization method of "constraint relaxation" is proposed. That is, let Γ_p includes all anticipated accidents first, i.e. $\Gamma_p = \Gamma$, calculate the total cost of coordinated control, and then eliminate the accident with the minimum SSD from Γ_p and incorporate it into Γ_c, re-conduct the inner-layer optimization and calculate the total cost of coordinated control to verify whether the total cost of coordinated control is reduced or not. If it is no longer decrease, the result of the previous step is the optimal scheme; if it continues to decrease, the accident with the minimum SSD in Γ_p will be eliminated and then incorporated into Γ_c to solve the inner-layer optimization. The above process will be repeated until the total cost no longer decreases.

The process of outer-layer optimization method based on "constraint relaxation" is shown in Figure 6. Assume that $\boldsymbol{x}_{\alpha,0}$ is the initial operation point, and there are only three anticipated accidents, i.e. $\Gamma = \{\lambda_1, \lambda_2, \lambda_3\}$, the corresponding SSRs are $\Omega(\lambda_1)$, $\Omega(\lambda_2)$, $\Omega(\lambda_2)$ respectively, the dispatching cost is represented by the norm of vector, the optimization process of "constraint relaxation" is mainly as follows:

Step 1: Let the preventive control subset include all anticipated accidents, i.e. $\Gamma_p = \Gamma = \{\lambda_1, \lambda_2, \lambda_3\}, \Gamma_c = \phi$.

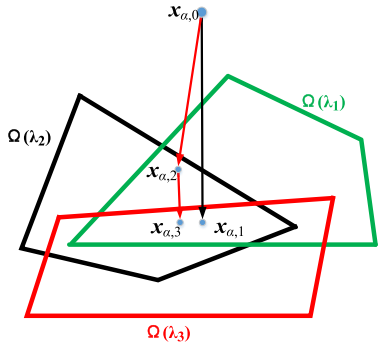

FIGURE 6. Schematic diagram of outer-layer optimization by constraint relaxation method.

Assume that the operation point after preventive control is $\boldsymbol{x}_{\alpha,1}$, satisfying the static security constraints of all anticipated accidents, while the accident λ_3 has the minimum SSD. In this case, the cost of coordinated control is $C_1 = |\overrightarrow{\boldsymbol{x}_{\alpha,0}\boldsymbol{x}_{\alpha,1}}|$, where $|\overrightarrow{\boldsymbol{x}_{\alpha,0}\boldsymbol{x}_{\alpha,1}}|$ denotes the cost of preventive control.

Step 2: Eliminate the anticipated accident λ_3 which has the minimum SSD from Γ_p and incorporate it into Γ_c, and judge whether λ_3 is a dominant accident, if not, then $\Gamma_p = \{\lambda_1, \lambda_2\}, \Gamma_c = \{\lambda_3\}$. If λ_3 is a dominant accident, re-incorporate the dominated accident into the preventive control subset Γ_p, then calculate the preventive control scheme for the preventive control subset Γ_p and the corrective control scheme for the accident λ_3. Assuming that λ_3 is not a dominant event, the total cost is $C_2 = |\overrightarrow{\boldsymbol{x}_{\alpha,0}\boldsymbol{x}_{\alpha,2}}| + (P(\lambda_3)|\overrightarrow{\boldsymbol{x}_{\alpha,2}\boldsymbol{x}_{\alpha,3}}| + C_r(\lambda_3))$, where $|\overrightarrow{\boldsymbol{x}_{\alpha,0}\boldsymbol{x}_{\alpha,2}}|$ denotes the cost of preventive control, $P(\lambda_3)$ denotes the probability of anticipated accident λ_3, $|\overrightarrow{\boldsymbol{x}_{\alpha,2}\boldsymbol{x}_{\alpha,3}}|$ denotes the dispatching cost of corrective control, and $C_r(\lambda_3)$ denotes the risk cost of corrective control.

Step 3: Compare the value of C_1 and C_2, if $C_1 \leq C_2$, the calculation result of step 1 is the optimal coordinated control scheme. Otherwise, continue to use the "constraint relaxation" method for the outer-layer optimization, eliminate the anticipated accident λ_2 with the minimum SSD from the preventive control subset Γ_p and incorporate it into the corrective control subset Γ_c, then return to step 2, and calculate the total cost of coordinated control again until the total cost of coordinated control no longer decreases.

Therefore, the flow chart of coordinated control is shown in Figure 7.

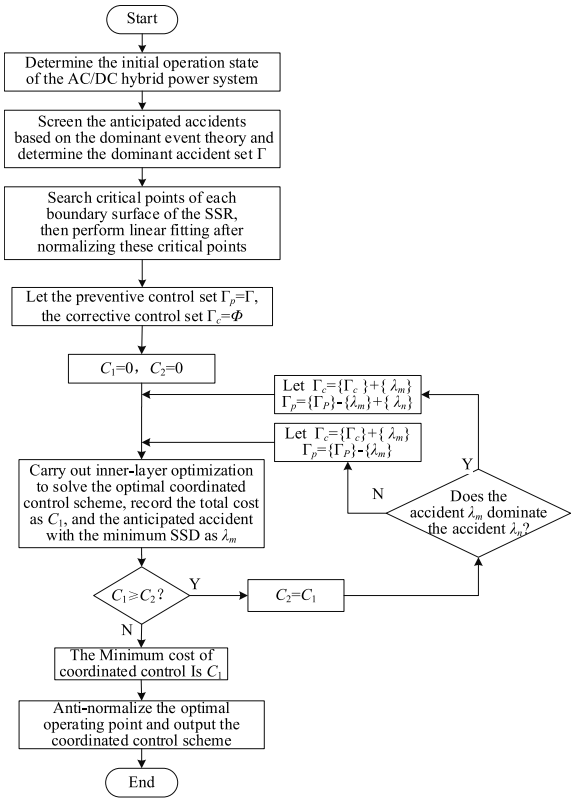

FIGURE 7. Flow chart of coordinated control.

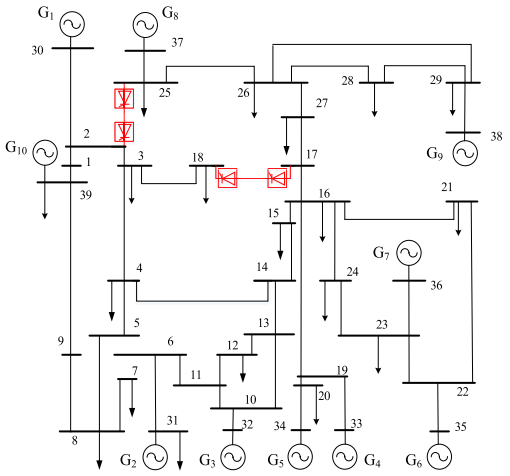

FIGURE 8. The topology of the transformed IEEE 39-node system.

V. CASE STUDY AND ANALYSIS

A. THE TRANSFORMED IEEE 39-NODE SYSTEM

In order to verify the effectiveness of the proposed method, this chapter takes the transformed IEEE 39-node system as an example to test the proposed method. The topology of the transformed IEEE 39-node system is shown in Figure 8. This AC/DC hybrid power system is formed by replacing the original AC lines with DC lines that transmit nearly the same power between the buses 25-2 and 17-18, respectively based on the standard topology. For the DC system, the rectifier-side uses constant-current control, and the inverter-side uses constant-voltage control. The referenced capacity is 100MW and the reference voltage is 345kV of the system.

In this paper, the generator of bus No. 31 is selected as the balance node and does not participate in the dispatch. The generators, loads of the remaining nodes, and the control variables of the DC line participate in the security control, so the SSR is a 60-dimensional geometry in Euclidean space. The initial operating points and constraints of the system control variables (corresponding to the dimension variables of the SSR) are shown in Appendix (Table 7), and

the AC line number and its active transmission limit are shown in Appendix (Table 8). The value range of the trigger angle α of the DC subsystem is $10° \leq \alpha \leq 45°$, and the value range of the extinction angle γ of the DC subsystem is $15° \leq \gamma \leq 35°$.

B. ANTICIPATED ACCIDENT SCREENING BASED ON DOMINANT EVENT THEORY

In a practical AC/DC hybrid power system, the probability of single faults is much greater than that of multiple faults, and in order to fully reflect the role of fast power flow transfer capability of the DC subsystem in maintaining the static security of the system, so only AC line break fault accidents considered in this paper. There are 26 anticipated accidents (the accidents that will cause the system to be islanded are not considered) before screening based on the theory of dominant event, as shown in Table 1. The subscript i in anticipated accident λ_i corresponding to the ID of line in Appendix (Table 8).

TABLE 1. The exceeding value caused by different anticipated accident.

Anticipated accident	Out-of-limit electrical quantity	Exceeding value/p.u.
λ_1, λ_2, λ_3, λ_5, λ_7, λ_9,λ_{10}, λ_{11}, λ_{14}, λ_{15}, λ_{16}, λ_{20}, λ_{21}, λ_{28}, λ_{34}, λ_{41}, λ_{42}, λ_{43}	none	0
λ_8	Upper limit of PF for line 6-11	1.2498
λ_{12}	Upper limit of PF for line 4-14	1.0107
	Upper limit of PF for line 10-13	0.174
	Upper limit of PF for line 13-14	0.3988
λ_{17}	Upper limit of PF for line 10-13	0.5
λ_{18}	Upper limit of PF for line 6-11	0.5728
	Upper limit of PF for line 10-11	0.5
λ_{22}	Upper limit of PF for line 6-11	1.5986
	Upper limit of PF for line 10-11	0.1744
λ_{27}	Upper limit of PF for line 23-24	0.8558
λ_{33}	Upper limit of PF for line 16-24	0.3003
	Upper limit of PF for line 22-23	0.5
	Upper limit of PF for line 23-24	3.5847
λ_{36}	Upper limit of PF for line 16-21	0.7948
	Upper limit of PF for line 21-22	0.6051

Each anticipated accident includes the upper and lower limits of node voltage, active output, active/reactive load, line power flow, and DC control quantities. There will be 120 security constraint boundary surfaces and 134 operation constraint boundary surfaces. The expressions of the security constraint boundary surface can be obtained directly, but when using the fitting method to calculate the operation constraint boundary surface expression, a large number of critical points need to be searched. If the number of critical points is 3 times more than of the dimension of the SSR, then more than 24120 critical points need to be searched for each anticipated accident, which is bound to be very large in computation.

In order to improve the optimization efficiency and simplify the optimization space of preventive control, the anticipated accidents are screened based on the theory of dominant event. Before the screening, the out-of-limit electrical quantity and exceeding value caused by each anticipated accident are shown in Table 1. In Table 1 the anticipated accidents without out-of-limit quantity can be dominated by any of the anticipated accidents with out-of-limit quantity, and the anticipated accident λ_{27} can be dominated by anticipated accident λ_{33}. So the number of valid anticipated accidents is reduced to 7 after screening, and the results before and after screening are shown in Table 2. It can be seen that the dominant event theory can effectively reduce the size of the anticipated accident set and the complexity of optimization space for preventive control.

TABLE 2. The screening results of anticipated accidents.

	Before screening	After screening
Anticipated accidents	λ_1, λ_2, λ_3, λ_5, λ_7, λ_8, λ_9, λ_{10}, λ_{11}, λ_{12}, λ_{14}, λ_{15}, λ_{16}, λ_{17}, λ_{18}, λ_{20}, λ_{21}, λ_{22}, λ_{27}, λ_{28}, λ_{33}, λ_{34}, λ_{36}, λ_{41}, λ_{42}, λ_{43}	λ_8, λ_{12}, λ_{17}, λ_{18}, λ_{22}, λ_{33}, λ_{36}
The NO. of anticipated accidents	26	7
Reduction rate	73.08%	

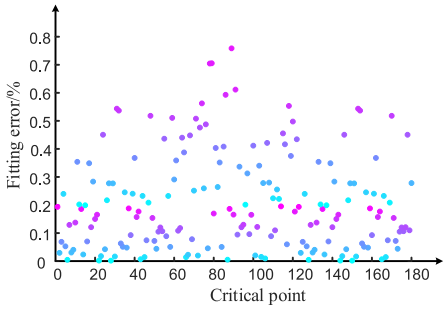

FIGURE 9. Fitting error of critical points of upper limit of transmission power of line 14-15 under normal operating condition.

C. SOLUTION OF OPTIMAL COORDINATED CONTROL STRATEGY

In order to ensure the operating point after preventive control meets the static security under normal operating conditions, the normal operating state is taken as a special case of the anticipated accidents set, that is, the anticipated accidents set is $\Gamma = \{\lambda_0, \lambda_8, \lambda_{12}, \lambda_{17}, \lambda_{18}, \lambda_{22}, \lambda_{33}, \lambda_{36}\}$, where λ_0 represents the normal operating state. The boundary surfaces of the dominant events are linearly fitted. The linear fitting coefficients of the boundary surfaces corresponding to the upper limit of the transmission power of line 14-15 under normal operation is shown in Appendix (Table 9), and the fitting errors of its 180 critical points are shown in Figure 9. It can be seen from the Figure 9 that the fitting errors are all below 5%, meeting the engineering error requirements,

and the fitting errors of the boundaries of the remaining boundary surfaces are all less than 5%, so it is feasible to use hyperplanes to represent these boundary surfaces of these SSRs.

When formulating the coordinated control scheme, because the cost of active output and voltage adjustment of the generator is relatively low, the unit adjustment cost weight coefficient is set as 5; The cost of load shedding is relatively larger, so the unit adjustment cost weight coefficient is set as 100; And the unit adjustment cost weight coefficient of DC control quantity is set as 1. At the same time, the safety margin is taken as $d_{\min} = 0.005$ in this paper. The probabilities of occurrence of anticipated accidents are shown in Appendix (Table 8). The line importance coefficient ω_m, as well as the node importance coefficient, ω_k are both set as 2500, the severity index factor of voltage out-of-limit e_v, as well as the severity index factor of power flow overload, e_l are both set as 1.1.

Only after 4 iterations, the optimal coordinated control scheme is obtained by applying the method proposed in this paper. The changes of different costs are shown in Figure 10 and the changes of anticipated accidents in preventive control subset Γ_p and corrective control subset Γ_c are shown in Table 3.

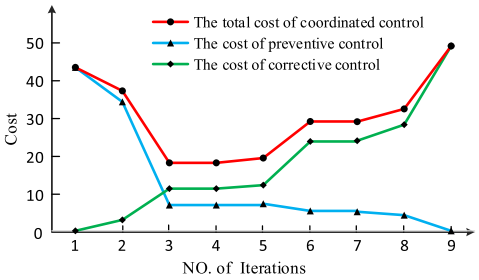

FIGURE 10. Cost changes during iteration.

TABLE 3. Change of anticipated accidents in preventive control subset and corrective control subset.

NO. of Iterations	Preventive control subset	Corrective control subset
1	$\lambda_0, \lambda_8, \lambda_{12}, \lambda_{17}, \lambda_{18}, \lambda_{22}, \lambda_{33}, \lambda_{36}$	$\emptyset$
2	$\lambda_0, \lambda_8, \lambda_{12}, \lambda_{17}, \lambda_{18}, \lambda_{33}, \lambda_{36}$	λ_{22}
3	$\lambda_0, \lambda_8, \lambda_{12}, \lambda_{17}, \lambda_{18}, \lambda_{27}, \lambda_{36}$	$\lambda_{22}, \lambda_{33}$
4	$\lambda_0, \lambda_8, \lambda_{12}, \lambda_{18}, \lambda_{27}, \lambda_{36}$	$\lambda_{17}, \lambda_{22}, \lambda_{33}$
5	$\lambda_0, \lambda_8, \lambda_{12}, \lambda_{27}, \lambda_{36}$	$\lambda_{17}, \lambda_{18}, \lambda_{22}, \lambda_{33}$
6	$\lambda_0, \lambda_8, \lambda_{27}, \lambda_{36}$	$\lambda_{12}, \lambda_{17}, \lambda_{18}, \lambda_{22}, \lambda_{33}$
7	$\lambda_0, \lambda_8, \lambda_{36}$	$\lambda_{12}, \lambda_{17}, \lambda_{18}, \lambda_{22}, \lambda_{27}, \lambda_{33}$
8	λ_0, λ_8	$\lambda_{12}, \lambda_{17}, \lambda_{18}, \lambda_{22}, \lambda_{27}, \lambda_{33}, \lambda_{36}$
9	λ_0	$\lambda_8, \lambda_{12}, \lambda_{17}, \lambda_{18}, \lambda_{22}, \lambda_{27}, \lambda_{33}, \lambda_{36}$

In the 3rd iteration, the λ_{33} in Γ_p is eliminated, so the λ_{27} dominated by λ_{33} needs to be added into Γ_p to participate in the iterative process of coordinated control starting from the 3rd iteration. It can be seen from the Figure 10 that, with the progress of the iteration process, the cost of preventive control becomes lower and lower. Finally, when the Γ_p only contains the normal operating state, i.e. $\Gamma_p = \{\lambda_0\}$, the cost of preventive control is 0, while the cost of corrective control increases from 0, and the total cost of coordinated control is obviously monotonic.

However, in the 3rd and 4th iterations, the costs of preventive control and the expected cost of corrective control are the same, and both have the lowest value. According to the network topology and system parameters, if the operating point can satisfy the static security requirements of λ_{18}, it must satisfy the static security requirements of λ_{17}. Therefore, it can be said that λ_{17} is dominated by λ_{18}. Thus during the 4th iteration, each cost remains unchanged. In this paper, it is considered that the optimal coordination control scheme can be obtained in the 4th iteration.

In the optimal coordinated control strategy, there are six anticipated accidents in the preventive control subset, i.e. $\Gamma_p = \{\lambda_0, \lambda_8, \lambda_{12}, \lambda_{18}, \lambda_{27}, \lambda_{36}\}$; in the corrective control subset, there are three anticipated accidents, i.e. $\Gamma_c = \{\lambda_{17}, \lambda_{22}, \lambda_{33}\}$. However, since λ_{17} is dominated by λ_{18}, there are only two anticipated accidents (λ_{17} and λ_{18}) insecurity after preventive control under the optimal coordinated control scheme. Therefore, it is necessary to formulate corresponding corrective control schemes for these two anticipated accidents. After the occurrence of these two anticipated accidents, the corresponding control schemes are applied to meet the static security requirement. Under the optimal coordinated control strategy, the control variables and their adjusted values involved in the preventive control scheme are shown in Figure 11. In $\Gamma_p = \{\lambda_0, \lambda_8, \lambda_{12}, \lambda_{18}, \lambda_{27}, \lambda_{36}\}$, the changes of electric quantities before and after preventive control are shown in Table 4; The corresponding corrective control schemes for each anticipated accident in Γ_c are shown in Table 5.

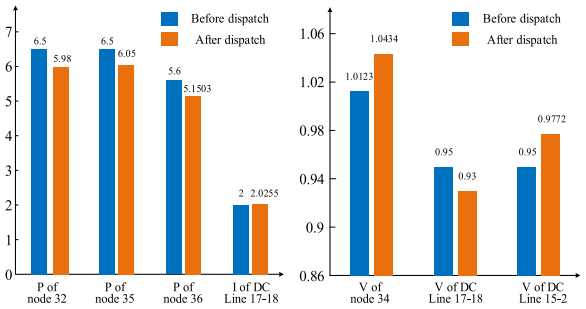

FIGURE 11. The changes variables involved in preventive control under the optimal coordinated control scheme.

In order to facilitate comparative analysis, Table 6 also gives the control cost comparison results of pure preventive control and pure corrective control. In the optimal solution process of optimal coordinated control, the result of the 1st iteration is the result of pure preventive control, and the dispatching scheme is shown in Figure 12.

It can be seen from Table 6 and Figure 12 that, due to the serious anticipated accidents (λ_{22} and λ_{33}) included in the anticipated accidents set Γ. In the pure preventive control, more adjustments are involved and the cost of preventive control is relatively high. In the 3rd iteration, λ_{22} and λ_{33} have been eliminated from the preventive control subset Γ_p and

TABLE 4. Change of electric quantity before and after preventive control.

Anticipated accident in preventive control subset	Electrical quantity	Upper limit/p.u.	Value before dispatching/p.u	Value after dispatching/p.u.
λ_8	PF of line 6-11	4.8	6.0498	4.5556
λ_{12}	PF of line 4-14	5	6.0107	4.5215
	PF of line 10-13	6	6.1740	5.6720
	PF of line 13-14	6	6.3988	5.8762
λ_{18}	PF of line 6-11	4.8	5.3728	4.6877
	PF of line 10-11	6	6.5000	5.9750
λ_{27}	PF of line 23-24	6	6.8558	5.9502
λ_{36}	PF of line 16-21	6	6.7948	5.8990
	PF of line 21-22	9	9.6051	8.6959

TABLE 5. Corrective control subset and control schemes.

Anticipated accident in corrective control subset	Corrective control measures set			Maximum limit before dispatching	SSD before dispatching	SSD after dispatching
	Control variable	Before dispatching	After dispatching			
λ_{22}	P of node 32	5.980	4.862	Upper transmission power of line 6-11	0.1234	-0.005
	P of node 33	5.151	5.417			
	V of DC line 17-18	0.930	0.865			
	V of DC line 25-2	0.977	0.941			
λ_{33}	P of node 32	5.980	7.877	Upper transmission power of line 23-24	0.2018	-0.005
	P of node 35	6.050	5.975			
	P of node 36	5.150	2.478			

TABLE 6. Control cost comparison of different control schemes.

Control schemes	Cost of preventive control	Expected cost of corrective control		Total cost
		Expected dispatching cost of corrective control	Risk cost	
Pure preventive control scheme	43.2081	0	0	43.2081
Pure corrective control scheme	0	0.0047	48.8487	48.8534
Coordinated control scheme	7.5332	0.0023	11.1449	18.6804

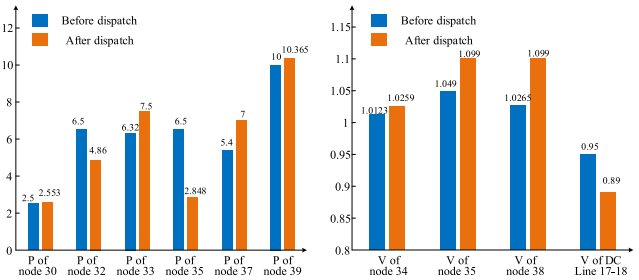

FIGURE 12. The changes of control variables involved in pure preventive control.

incorporated into the corrective control subset Γ_c, therefore, the cost of preventive control drops significantly, while the cost of corrective control increases significantly.

In terms of optimal solution time, the traditional simulation method was used in [30] to calculate the optimal corrective control scheme for one single anticipated accident of the test system similar to Figure 8, which takes about 2 minutes. However, based on the method proposed in this paper, the optimal corrective control scheme for one anticipated accident in the corrective control subset Γ_p can be solved in 1 second, and the optimal coordinated control scheme for the anticipated accident set Γ can be solved in 6 seconds. And the current optimization program is only written in MATLAB to verify the algorithm. If it is written in C as a practical software, there is still a lot of room to improve the calculation speed, and it is expected to be used online. What is more, when the number of anticipated accidents continues to increase, the advantages of this method will become more apparent.

VI. CONCLUSION

Preventive control and corrective control have strong complementarity to each other, which are two important methods to maintain the security operation of AC/DC hybrid power system. For a long time, the research on the relationship between them has been separated. The optimization and coordination between them is extremely important to ensure the safe and economic operation of AC/DC hybrid power system.

In this paper, based on the SSR of AC/DC hybrid power system, a two-layer optimization algorithm of coordinated control between preventive control and corrective control is proposed, which takes the minimum cost of coordinated control as the objective function. Compared with the existing research, this paper adopts three measures to improve the efficiency of calculating the coordinated control scheme: Firstly, based on the dominant event, the invalid anticipated accidents are eliminated to reduce the scale of the model; Secondly, for the two-layer optimization problem with dynamic constraints, an outer-layer optimization method based on "constraint relaxation" method is proposed, which effectively avoids the "curse of dimensionality" problem caused by exhaustive method; Finally, in the process of inner-layer optimization, the linear expressions of the boundary surfaces

TABLE 7. The initial operating point and upper and lower limits of control variables.

Sequence NO.	Control variable	Initial operating point /p.u.	Upper limit /p.u.	Lower limit /p.u.	Sequence NO.	Control variable	Initial operating point /p.u.	Upper limit /p.u.	Lower limit /p.u.
1	P of node 1	0.976	0.976	0	31	P of node 26	1.39	1.39	0
2	Q of node 1	0.442	0.442	0	32	Q of node 26	0.17	0.17	0
3	P of node 3	3.22	3.22	0	33	P of node 27	2.81	2.81	0
4	Q of node 3	0.024	0.024	0	34	Q of node 27	0.755	0.755	0
5	P of node 4	5	5	0	35	P of node 28	2.06	2.06	0
6	Q of node 4	1.84	1.84	0	36	Q of node 28	0.276	0.276	0
7	P of node 7	2.338	2.338	0	37	P of node 29	2.835	2.835	0
8	Q of node 7	0.84	0.84	0	38	Q of node 29	0.269	0.269	0
9	P of node 8	5.22	5.22	0	39	V of node 30	1.0499	1.1	0.9
10	Q of node 8	1.766	1.766	0	40	P of node 30	2.5	3.5	1.05
11	P of node 9	0.065	0.065	0	41	V of node 32	0.9841	1.1	0.9
12	Q of node 9	-0.666	-0.666	0	42	P of node 32	6.5	8	3.4
13	P of node 12	0.0853	0.0853	0	43	V of node 33	0.9972	1.1	0.9
14	Q of node 12	0.88	0.88	0	44	P of node 33	6.32	7.5	2.25
15	P of node 15	3.2	3.2	0	45	V of node 34	1.0123	1.1	0.9
16	Q of node 15	1.53	1.53	0	46	P of node 34	5.08	6.5	1.95
17	P of node 16	3.29	3.29	0	47	V of node 35	1.0494	1.1	0.9
18	Q of node 16	0.323	0.323	0	48	P of node 35	6.5	7.5	2.25
19	P of node 18	1.58	1.58	0	49	V of node 36	1.0636	1.1	0.9
20	Q of node 18	0.3	0.3	0	50	P of node 36	5.6	7.5	2.25
21	P of node 20	6.8	6.8	0	51	V of node 37	1.0275	1.1	0.9
22	Q of node 20	1.03	1.03	0	52	P of node 37	5.4	7	2.1
23	P of node 21	2.74	2.74	0	53	V of node 38	1.0265	1.1	0.9
24	Q of node 21	1.15	1.15	0	54	P of node 38	8.3	9	3
25	P of node 23	2.475	2.475	0	55	V of node 39	1.03	1.1	0.9
26	Q of node 23	0.846	0.846	0	56	P of node 39	10	13	3.5
27	P of node 24	3.086	3.086	0	57	DC current of 17-18	2	2.75	0.5
28	Q of node 24	-0.922	-0.922	0	58	DC voltage of 17-18	0.85	1.2	0.85
29	P of node 25	2.24	2.24	0	59	DC current of 25-2	2.5	3.3	0.6
30	Q of node 25	0.472	0.472	0	60	DC voltage of 25-2	0.85	1.2	0.85

TABLE 8. Ac line ID and its active power transmission limit.

Line ID	Line NO.	Power flow limit/p.u.	Failure probability /$\times 10^{-2}$	Line ID	Line NO.	Power flow limit/p.u.	Failure probability /$\times 10^{-2}$
1	1-2	6	1.250	23	14-15	6	0.840
2	1-39	10	2.000	24	15-16	6	0.655
3	2-3	5	1.210	25	16-17	6	1.080
4	2-30	9	0.850	26	16-19	6	1.050
5	3-4	5	1.700	27	16-21	6	1.250
6	3-18	5	0.320	28	16-24	6	0.150
7	4-5	6	1.220	29	17-27	6	0.830
8	4-14	5	1.040	30	19-20	9	0.350
9	5-6	12	2.210	31	19-33	9	0.750
10	5-8	9	1.900	32	20-34	9	0.842
11	6-7	9	1.740	33	21-22	9	0.720
12	6-11	4.8	2.660	34	22-23	6	1.920
13	6-31	18	0.560	35	22-35	9	0.800
14	7-8	9	1.370	36	23-24	6	1.960
15	8-9	9	1.120	37	23-36	9	0.580
16	9-39	9	2.100	38	25-26	6	1.060
17	10-11	6	2.340	39	25-37	9	0.840
18	10-13	6	2.350	40	26-27	6	1.120
19	10-32	9	0.360	41	26-28	6	2.790
20	12-11	5	1.820	42	26-29	6	2.100
21	12-13	5	1.256	43	28-29	6	1.510
22	13-14	6	0.810	44	29-38	12	0.880

of SSR are used instead of the nonlinear power flow equations as the security constraint, which improves the efficiency of optimal solution greatly. At last, through the analysis and calculation of the transformed IEEE 39-node AC/DC hybrid power system, the solution efficiency is improved greatly, which provides the possibility for online application.

TABLE 9. Linear fitting coefficient of part boundary surfaces of anticipated accident λ_0.

Sequence NO.	Dimension of SSR	The upper limit of power flow of line 14-15	Sequence NO.	Dimension of SSR	The upper limit of power flow of line 14-15
1	P of node 1	-0.00043	31	P of node 26	0.50045
2	Q of node 1	0.00044	32	Q of node 26	-0.00262
3	P of node 3	0.00203	33	P of node 27	1.01399
4	Q of node 3	0.00164	34	Q of node 27	-0.00206
5	P of node 4	0.00251	35	P of node 28	0.73678
6	Q of node 4	0.00644	36	Q of node 28	-0.00117
7	P of node 7	0.00135	37	P of node 29	1.00612
8	Q of node 7	0.00283	38	Q of node 29	-0.00075
9	P of node 8	0.00184	39	V of node 30	0.00242
10	Q of node 8	0.00405	40	P of node 30	-0.00234
11	P of node 9	-0.00088	41	V of node 32	-0.00268
12	Q of node 9	0.00157	42	P of node 32	-0.00284
13	P of node 12	0.00173	43	V of node 33	-0.00064
14	Q of node 12	-0.00005	44	P of node 33	-2.19771
15	P of node 15	1.13731	45	V of node 34	-0.00340
16	Q of node 15	0.00269	46	P of node 34	-1.77150
17	P of node 16	1.17276	47	V of node 35	-0.00558
18	Q of node 16	-0.00090	48	P of node 35	-2.28160
19	P of node 18	0.00358	49	V of node 36	-0.00420
20	Q of node 18	0.00105	50	P of node 36	-1.95441
21	P of node 20	2.39393	51	V of node 37	-0.00219
22	Q of node 20	0.00181	52	P of node 37	-1.92036
23	P of node 21	0.96934	53	V of node 38	-0.00092
24	Q of node 21	0.00228	54	P of node 38	-2.90802
25	P of node 23	0.86880	55	V of node 39	0.00061
26	Q of node 23	0.00149	56	P of node 39	-0.00656
27	P of node 24	1.09860	57	DC current of 17-18	0.39265
28	Q of node 24	0.00128	58	DC voltage of 17-18	0.12034
29	P of node 25	0.80253	59	DC current of 25-2	0.47224
30	Q of node 25	-0.00234	60	DC voltage of 25-2	0.15889

In this paper, the influence of weather conditions and load rate on the forced outage of components is ignored, and the fault probability model is relatively simple. In the future work, the load rate and weather factors should be taken into account to establish a detailed transmission line fault model. Besides, in the actual power system, there is still the possibility of multiple failures, so in the future research, the static security constraints of multiple faults should also be taken into account in order to obtain the optimal coordinated control strategy to meet the actual operation of the system.

APPENDIX

See Tables 7–9.

REFERENCES

[1] S. A. Siddiqui, K. Verma, K. R. Niazi, and M. Fozdar, "A unified control scheme for power system transient stability enhancement through preventive and emergency control," *Int. Trans. Electr. Energy Syst.*, vol. 26, no. 2, pp. 365–383, Feb. 2016.

[2] A. Dhandhia, V. Pandya, and P. Bhatt, "Multi-class support vector machines for static security assessment of power system," *Ain Shams Eng. J.*, vol. 11, no. 1, pp. 57–65, 2019.

[3] T. Venkatesh and T. Jain, "Synchronized measurements-based wide-area static security assessment and classification of power systems using case based reasoning classifiers," *Comput. Electr. Eng.*, vol. 68, pp. 513–525, May 2018.

[4] H. Yang, W. Zhang, J. Chen, and J. Xie, "Optimal coordinated voltage control of AC/DC power systems for voltage stability enhancement," *Int. J. Electr. Power Energy Syst.*, vol. 108, pp. 252–262, Jun. 2019.

[5] K. Jiang, Y. Zhang, Y. Li, and J. Yang, "The prevention-correction coordinated control of power system based on operational risk," in *Proc. Chin. Autom. Congr. (CAC)*, Nov. 2015, pp. 1355–1360.

[6] Y. Zhou, J. Wu, L. Ji, Z. Yu, K. Lin, and L. Hao, "Transient stability preventive control of power systems using chaotic particle swarm optimization combined with two-stage support vector machine," *Electr. Power Syst. Res.*, vol. 155, pp. 111–120, Feb. 2018.

[7] G. Li and S. M. Rovnyak, "Integral square generator angle index for stability ranking and control," *IEEE Trans. Power Syst.*, vol. 20, no. 2, pp. 926–934, May 2005.

[8] D. Gan, R. J. Thomas, and R. D. Zimmerman, "Stability-constrained optimal power flow," *IEEE Trans. Power Syst.*, vol. 15, no. 2, pp. 535–540, May 2000.

[9] D. Ruiz-Vega and M. Pavella, "A comprehensive approach to transient stability control part 1: Near optimal preventive control," in *Proc. IEEE Power Eng. Soc. Gen. Meeting*, Jul. 2003, p. 1810.

[10] Z. Wang, X. Song, and Z. Yang, "A coordinated preventive and emergency control considering system transient security," *Proc. CSEE*, vol. 34, no. 34, pp. 6159–6166, Dec. 2014.

[11] X. Fu, "Hybrid control of power system static security," *Electr. Power Autom. Equip.*, vol. 37, no. 1, pp. 124–130, 2017.

[12] S. Jiang, J. Yang, and J. Wang, "Defense strategy against large power grid cascading failure based on coordinated preventive-emergency control," *Electr. Power Autom. Equip.*, vol. 39, no. 12, pp. 148–154, 2019.

[13] K. Verma and K. R. Niazi, "A coherency based generator rescheduling for preventive control of transient stability in power systems," *Int. J. Electr. Power Energy Syst.*, vol. 45, no. 1, pp. 10–18, Feb. 2013.

[14] K. Alzaareer, M. Saad, H. Mehrjerdi, C. Z. El-Bayeh, D. Asber, and S. Lefebvre, "A new sensitivity approach for preventive control selection in real-time voltage stability assessment," *Int. J. Electr. Power Energy Syst.*, vol. 122, Nov. 2020, Art. no. 106212.
[15] S. J. Chen, Q. X. Chen, Q. Xia, and C. Q. Kang, "Steady-state security assessment method based on distance to security region boundaries," *IET Gener., Transmiss. Distrib.*, vol. 7, no. 3, pp. 288–297, Mar. 2013.
[16] S. Chen, Q. Chen, Q. Xia, H. Zhong, and C. Kang, "N - 1 security assessment approach based on the steady-state security distance," *IET Gener., Transmiss. Distrib.*, vol. 9, no. 15, pp. 2419–2426, Nov. 2015.
[17] Y. Yu, Y. Liu, C. Qin, and T. Yang, "Theory and method of power system integrated security region irrelevant to operation states: An introduction," *Engineering*, vol. 6, no. 7, pp. 754–777, Jul. 2020.
[18] Y. Yu, D. Wang, and C. Wang, "Framework of security region based probabilistic security assessment for power transmission system," *J. Tianjin Univ.*, vol. 40, no. 6, pp. 699–703, 2007.
[19] Y. Liu and Y. Yu, "Probabilistic steady-state and dynamic security assessment of power transmission system," *Sci. China Technol. Sci.*, vol. 56, no. 5, pp. 1198–1207, May 2013.
[20] T. Yang and Y. Yu, "Steady-state security region-based voltage/var optimization considering power injection uncertainties in distribution grids," *IEEE Trans. Smart Grid*, vol. 10, no. 3, pp. 2904–2911, May 2019.
[21] J. S. Ferreira, E. J. de Oliveira, A. N. de Paula, L. W. de Oliveira, and J. A. P. Filho, "Optimal power flow with security operation region," *Int. J. Electr. Power Energy Syst.*, vol. 124, Jan. 2021, Art. no. 106272.
[22] Z. Chen, J. Yan, and Z. Zhu, "Characterization and application of decoupling security region in multi-infeed AC/DC hybrid system," *Autom. Electr. Power Syst.*, vol. 44, no. 22, pp. 37–44, 2020.
[23] T. Yang and Y. Yu, "Security region-based laminar flow coordinated optimization of grids," *Int. J. Electr. Power Energy Syst.*, vol. 124, Jan. 2021, Art. no. 106406.
[24] Y. Yu and W. Luan, "Practical dynamic security regions of power systems," *Proc. CSEE*, vol. 10, no. S1, pp. 24–30, 1990.
[25] H. D. Liu, A. Chang, Q. Li, Z. X. Li, W. Feng, and N. Q. Han, "A directional rapid search method in PDSR based on the fitting method," *Adv. Mater. Res.*, vols. 694–697, pp. 2989–2992, May 2013.
[26] Y.-L. Liu, X.-J. Shi, and Y. Xu, "A hybrid data-driven method for fast approximation of practical dynamic security region boundary of power systems," *Int. J. Electr. Power Energy Syst.*, vol. 117, May 2020, Art. no. 105658.
[27] Y. Wu, "Nonlinear speed control for a permanent magnet synchronous generator and the boost-chopper converter," *Trans. China Electrotech. Soc.*, vol. 29, no. S1, pp. 374–383, 2014.
[28] S. Cong, Z. Shang, and W. Tao, "An improved method of static security preventive control in power systems," *J. North China Electr. Power Univ.*, vol. 44, no. 1, pp. 24–30,38, 2017.
[29] S. Zhong, X. Han, and D. Liu, "Benders decomposition algorithm for corrective security-constrained optimal power flow," *Proc. CSEE*, vol. 31, no. 1, pp. 65–71, 2011.
[30] Z. Zhu, J. Yan, C. Lu, Z. Chen, and J. Tian, "Two-stage coordinated control strategy of AC/DC hybrid power system based on steady-state security region," *IEEE Access*, vol. 8, pp. 139221–139243, 2020.

ZHONG CHEN (Member, IEEE) received the M.S. and Ph.D. degrees from the School of Electrical Engineering, Southeast University, China, in 2002 and 2006, respectively. He is currently a Full Professor with the School of Electrical Engineering, Southeast University. His research interests include AC/DC power system stability analysis and control, electrical vehicle, renewable energy, and intelligent power technology.

JUN YAN (Student Member, IEEE) received the B.S. degree from the College of Electrical and Information Engineering, Hunan University, China, in 2018. He is currently pursuing the master's degree with the School of Electrical Engineering, Southeast University, China. His research interests include AC/DC power system operation analysis and control.

CHEN LU (Student Member, IEEE) received the B.S. degree from the School of Electrical Engineering, Sichuan University, China, in 2018. He is currently pursuing the master's degree with the School of Electrical Engineering, Southeast University, China. His research interests include AC/DC power system operation analysis and control.